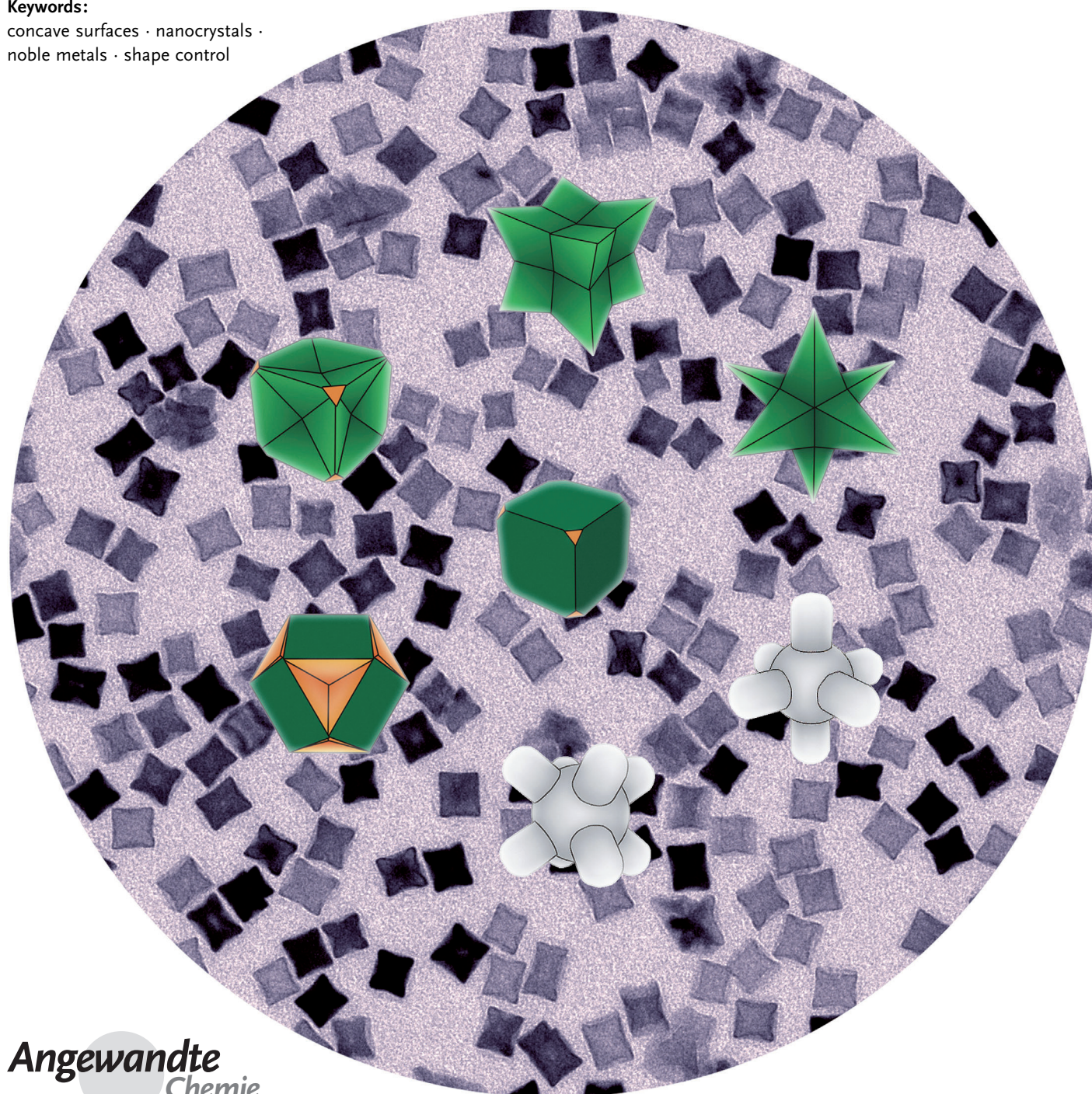


# Noble-Metal Nanocrystals with Concave Surfaces: Synthesis and Applications

Hui Zhang, Mingshang Jin, and Younan Xia\*

**Keywords:**

concave surfaces · nanocrystals ·  
noble metals · shape control





**M**etal nanocrystals with concave surfaces are interesting for a wide variety of applications that are related to catalysis, plasmonics, and surface-enhanced spectroscopy. This interest arises from their high-index facets, surface cavities, and sharp corners/edges. Two major challenges are associated with this novel class of nanocrystals: 1) how to generate a concave surface with negative curvature, which is not favored by thermodynamics owing to its higher energy than the convex counterpart; and 2) how to stabilize the morphology of a nanocrystal with concave structures on the surface. Recently, a number of different procedures have been developed for the synthesis of noble-metal nanocrystals with concave surfaces. This Review provides a brief account of these developments, with the aim of offering new insights into the growth mechanisms. We focus on methods based on two general strategies: 1) site-specific dissolution through etching and galvanic replacement; and 2) directionally controlled overgrowth by facet-selective capping, kinetic control, and template-directed epitaxy. Their enhanced catalytic and electrocatalytic properties are also described.

## From the Contents

<b>1. Introduction</b>	7657
<b>2. Two Different Synthetic Approaches to Concave Nanocrystals</b>	7658
<b>3. Concave Nanocrystals by Site-Specific Dissolution</b>	7661
<b>4. Concave Nanocrystals by Directionally Controlled Overgrowth</b>	7663
<b>5. Catalytic Properties and Related Applications</b>	7670
<b>6. Summary and Outlook</b>	7671

## 1. Introduction

The properties of a nanocrystal are determined by a set of parameters, such as composition, size, shape, morphology, and structure (solid versus hollow).<sup>[1–3]</sup> By tuning these parameters, the properties of a nanocrystal-based material can, in principle, be tailored to enhance its performance in a specific application. In recent years, shape control has received the greatest attention in exploration of nanocrystals made of noble metals (as well as many other types of inorganic materials). Controlling the shape of a nanocrystal may initially seem like a scientific curiosity, but its impact goes far beyond aesthetic appeal. For example, the shape of a Ag or Au nanocrystal determines its localized surface plasmon resonance (LSPR) properties and its merit in applications such as surface-enhanced Raman scattering (SERS).<sup>[4]</sup> The shape also controls the facet(s) and thus surface structure(s) of a metal nanocrystal, as well as the fractions of atoms at corners and edges.<sup>[5,6]</sup> All of these features are essential to applications in heterogeneous catalysis. Thanks to the efforts from many research groups, a large number of different shapes have now been reported for metal nanocrystals, with notable examples including cube, octahedron, tetrahedron, cuboctahedron, decahedron, icosahedron, bipyramid, plate, disk, bar, rod, and wire.<sup>[7,8]</sup> As a major limitation, all these nanocrystals are polyhedrons encased by convex surfaces.

Compared to the enormous success for shape-controlled synthesis of nanocrystals with convex surfaces, synthesis of nanocrystals with a concave surface is still in a very early stage of development. A concave structure suggests curving in or hollowed inward from the surface and thus presence of regions with negative curvature. For a two-dimensional system, a concave structure can be defined as a polygon that has at least one interior angle that is greater than 180 degrees. The same concept can be extended to a three-

dimensional system by focusing on the cross-sections. In general, high-index facets other than {100}, {110}, and {111} are involved in the construction of a concave surface. Owing to the high-index facets and negative curvature, nanocrystals with concave surfaces are expected to show unexplored or substantially enhanced properties relative to their convex counterparts.<sup>[9–12]</sup> The high-index facets, for example, have been shown with significantly enhanced activity for a number of catalysts based on noble metals owing to the presence of atomic steps and kinks with low coordination numbers in high densities.<sup>[13,14]</sup> It should be pointed out that nanostructures with branched arms on the surface naturally have concave regions on the surface.<sup>[15]</sup> Here we limit our discussion to single-crystal systems where the branched arms are epitaxially grown from different facets of the polyhedral cores.

In recent years, a large number of synthetic methods have been developed for generating concave nanocrystals of noble metals, including Ag, Au, Pd, Pt, Rh, as well as their bimetallic combinations. These methods can be divided into two complementary strategies: site-specific dissolution and directionally controlled overgrowth. When dissolution occurs on

[\*] Prof. Y. Xia  
The Wallace H. Coulter Department of Biomedical Engineering  
Georgia Institute of Technology and Emory University  
School of Chemistry and Biochemistry  
Georgia Institute of Technology, Atlanta, GA 30332 (USA)  
E-mail: younan.xia@bme.gatech.edu

Dr. H. Zhang  
State Key Laboratory of Silicon Materials  
Department of Materials Science and Engineering  
Zhejiang University, Hangzhou, Zhejiang 310027 (P.R. China)

Dr. M. Jin  
Center for Materials Chemistry  
Frontier Institute of Science and Technology  
Xi'an Jiaotong University, Xi'an, Shanxi 710049 (P.R. China)

the surface of a nanocrystal in an inhomogeneous pattern, the region experiencing faster dissolution will evolve into a concave structure. As for overgrowth, it is impossible to generate a concave structure from the perspective of thermodynamics. The Gibbs free energy of a concave region is always lower than that of a flat or convex region, resulting in preferential or faster growth for the concave region and thus elimination of a concave structure to help minimize the total surface energy.<sup>[16]</sup> In this case, the use of a capping agent, a template, and/or kinetic control has to be relied upon to generate nanocrystals with concave surfaces.

In this Review, we begin with a brief discussion on the types of possible concave nanocrystals that can be obtained using approaches based on dissolution and overgrowth. We then examine recent progress in the experimental implementation of these synthetic approaches, with a focus on the following methods: site-specific etching, galvanic replacement, facet-selective capping, kinetically-controlled overgrowth, and template-directed epitaxy. Finally, we present a few examples to show some of the unique and key properties of metal nanocrystals with concave surfaces for applications in both catalysis and electrocatalysis.

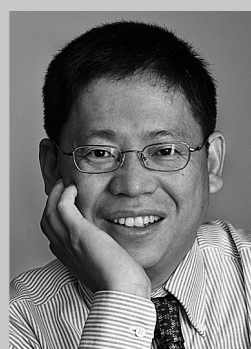
## 2. Two Different Synthetic Approaches to Concave Nanocrystals

Dissolution and overgrowth are two complementary approaches to the synthesis of nanocrystals with concave surfaces. For the purpose of simplicity, both approaches can be considered to start from a convex nanocrystal encased by a set of low-index facets, such as {100}, {110}, and {111}. The difference in dissolution or overgrowth rates for different crystallographic planes plays an important role in determining the final shape or morphology taken by the product. As noble-metal nanocrystals are typically synthesized in air and the reaction solutions often contain halide ions, such as  $\text{Cl}^-$  and  $\text{Br}^-$ , nanocrystals with twin defects (for example, bipyramids, decahedrons, and icosahedrons) can hardly survive owing to the involvement of oxidative etching caused by the halide ions and  $\text{O}_2$ .<sup>[17–19]</sup> As such, we only

focus on the formation of possible concave nanocrystals from single-crystal polyhedrons, such as cube, octahedron, and tetrahedron, that are slightly truncated at corners and therefore enclosed by a mix of {100} and {111} facets. These polyhedral nanocrystals can serve as templates for site-specific dissolution or as seeds for overgrowth to generate nanocrystals with concave structures on the surface.

The shape or morphology taken by the product evolving from a convex polyhedron is determined by the difference in dissolution or growth rates of three crystallographic planes: {100}, {110}, and {111}. There are seven different combinations for these dissolution or growth rates, with the following facet(s) being in dominance: {100}, {110}, {111}, {100} + {110}, {100} + {111}, {110} + {111}, and {100} + {110} + {111}. In practice, only four of these combinations—{100}, {111}, {100} + {110}, and {110} + {111}—will lead to the formation of nanocrystals with concave surfaces. The other three will be either too difficult to achieve experimentally or will result in the formation of nanocrystals with convex surfaces.

Table 1 shows the possible concave nanocrystals that could be prepared by site-specific dissolution. Starting from a cubic nanocrystal with slight truncation at corners, a concave cube could be obtained by preferentially forming pits on all of the six {100} faces. The preferential pitting may also take place at the eight corner sites or {111} faces, leading to the formation of a concave cuboctahedron with a large portion of {100} facets. Octapods and hexapods with concave surfaces will be formed if pitting occurs preferentially on {100} + {110} and {110} + {111} facets, respectively. Compared to a truncated cube, a truncated octahedron shares the same symmetry, although they have different ratios between the areas of {100} and {111} facets. As a result, the concave nanocrystals derived from a truncated octahedron should resemble those derived from a truncated cube, except for the difference in the proportion of various facets exposed on the surface. In contrast, a truncated tetrahedron can evolve into different shapes through selective dissolution. In this case, a truncated tetrahedron can be excavated on the {111} faces, resulting in the formation of a concave tetrahedron. Furthermore, a tetrapod with a concave surface will be generated by selective dissolution on both {100} and {110} facets.



Younan Xia was born in Jiangsu, China in 1965. He received a B.S. from the University of Science and Technology of China in 1987, a M.S. from the University of Pennsylvania in 1993, and a Ph.D. in Physical Chemistry from Harvard University (with Prof. George M. Whitesides) in 1996. He started as an Assistant Professor of Chemistry at the University of Washington (Seattle) in 1997, and was promoted to Associated Professor (2002) and Professor (2004). He joined Washington University in St. Louis in 2007 as the James M. McKelvey Professor for Advanced Materials. At the beginning of 2012, he moved to the Georgia Institute of Technology as the Brock Family Chair and GRA Eminent Scholar in Nanomedicine. His research interests include nanomaterials, biomaterials, nanomedicine, regenerative medicine, electrospinning, and colloidal science.



Hui Zhang was born in Zhejiang, China in 1977. He studied Materials Science at Zhejiang University (B.S. 1995, Ph.D. 2005). He started as a Lecturer in the Department of Materials Science and Engineering at Zhejiang University in 2005 and was promoted to Associate Professor in 2006. He then spent two years in Prof. Xia's group as a visiting scholar from 2009–2011. His current research interests include synthesis and application of noble-metal nanostructures.

**Table 1:** Possible concave nanocrystals that could be synthesized by site-specific dissolution of cubes, octahedrons, and tetrahedrons (all of them have slight truncation at corners).

Dissolution sites	Cubes	Octahedrons	Tetrahedrons
	concave cubes	concave truncated octahedron	
$\langle 100 \rangle$			
	concave cuboctahedron	concave octahedron	concave tetrahedron
$\langle 111 \rangle$			
	octapod	octapod	tetrapod
$\langle 100 \rangle + \langle 110 \rangle$			
	hexapod	hexapod	
$\langle 110 \rangle + \langle 111 \rangle$			

The two approaches based on overgrowth and dissolution should have similar outcomes except for the types of facets involved owing to a complementary relationship. As such, all the concave nanocrystals formed through dissolution can also

be produced by overgrowth by manipulating the growth rates of different planes (Table 2). For instance, a concave cube can be obtained through preferential overgrowth on both  $\{110\}$  and  $\{111\}$  facets, corresponding to selective dissolution on  $\{100\}$  facets. In general, concave nanocrystals prepared using a dissolution-based method are made of structures with a rounded profile rather than faceted structures typical of an overgrowth process, resulting in the formation of concave nanocrystals with the same symmetry but different shapes or morphologies. For example, when slightly truncated cubes or octahedrons were used as templates for site-specific dissolution on  $\{100\}$  and  $\{110\}$  facets, concave octapods with arms in a rounded profile were obtained.<sup>[20]</sup> In comparison, preferential overgrowth on  $\{111\}$  facets resulted in the formation of concave octapods with a polyhedral structure, known as concave trisoctahedrons, when the same cubes or octahedrons were used as seeds.<sup>[21]</sup>

The past several years have witnessed rapid and significant progress in the synthesis of noble-metal nanocrystals with concave surfaces. Table 3 shows a summary of such

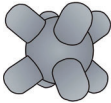
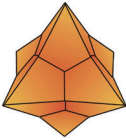
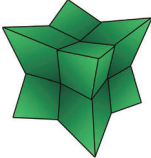
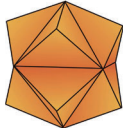
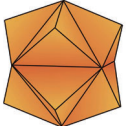
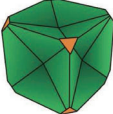
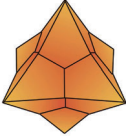
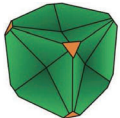
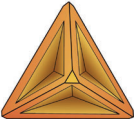
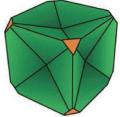
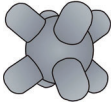
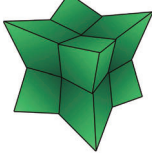
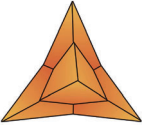
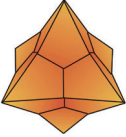
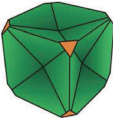
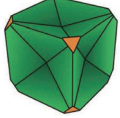
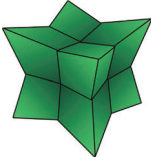
**Table 2:** Possible concave structures that could be obtained by seeded overgrowth along specific directions on different types of seeds: cubes, octahedrons, and tetrahedrons with slight truncation at corners.

Overgrowth Directions	Cubes	Octahedrons	Tetrahedrons
	hexapod	hexapod	
$\langle 100 \rangle$			
	octapod	trisoctahedron	tetrapod
$\langle 111 \rangle$			
	concave cuboctahedron	concave octahedron	concave tetrahedron
$\langle 100 \rangle + \langle 110 \rangle$			
	concave cube	concave truncated octahedron	
$\langle 110 \rangle + \langle 111 \rangle$			




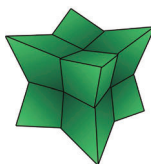
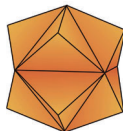
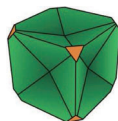
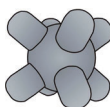
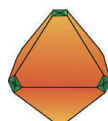
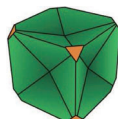
Mingshang Jin was born in Zhejiang, China in 1984. He received a B.S. degree in Chemistry (2006) and a Ph.D. degree in Physical Chemistry (2012) from Xiamen University with Prof. Zhaoxiong Xie. He was a visiting graduate student in Prof. Xia's group from 2009–2011. At the beginning of 2012, he started as a Professor of Materials Chemistry at Xi'an Jiaotong University, China. His research interests include the design and synthesis of metal nanomaterials for fuel cells, catalytic converters, and water-splitting devices.

**Table 3:** Summary of concave nanocrystals that have been successfully synthesized using site-specific etching, galvanic replacement, facet-selective capping, kinetically-controlled overgrowth, and template-directed epitaxy for a number of noble metals, including Ag, Au, Pd, Pt, and Rh, as well as their bimetallic combinations.

Metal	Approach	Concave nanocrystals			References
Ag	site-specific etching				[20]
Ag	kinetically controlled overgrowth				[21]
Au	facet-selective capping				[22–24]
Au	kinetically controlled overgrowth				[25]
Pd	site-specific etching				[26]
Pd	facet-selective capping				[27]
Pd	kinetically controlled overgrowth				[28]
Pt	site-specific etching				[29, 30]
Pt	facet-selective capping				[31]
Pt	kinetically controlled overgrowth				[32, 33]
Rh	kinetically controlled overgrowth				[34]



**Table 3:** (Continued)

Metal	Approach	Concave nanocrystals			References
Au/Pd	kinetically controlled overgrowth				[35, 36]
Au/Pd	template-directed epitaxial deposition				[37, 38]
Pd/Pt	galvanic replacement				[39]
Pt/Rh	kinetically controlled overgrowth				[34]

concave nanocrystals made of Ag, Au, Pd, Pt, and Rh, as well as their bimetallic combinations. In the following sections, we will discuss how these concave nanocrystals have been prepared experimentally, with an emphasis on mechanistic understanding and possible control. This discussion is also expected to shed light on the synthesis of concave nanocrystals made of other metals and even other types of inorganic materials.

### 3. Concave Nanocrystals by Site-Specific Dissolution

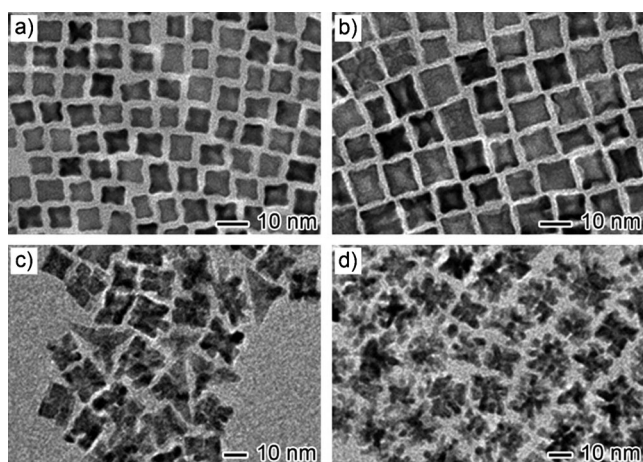
The dissolution of a metal is also widely known as corrosion, which is a common phenomenon that can lead to surface degradation and structure failure.<sup>[40]</sup> Corrosion may take place in many different forms, such as pitting, etching, galvanic replacement, and dealloying. It typically involves electrochemical reactions between the metal and its surroundings, and is governed by a set of parameters, such as redox potential, pH value, temperature, and ionic species. In general, corrosion is not a desirable process because of its damage to a surface or material. However, the concept of corrosion can be exploited to facilitate the formation of nanocrystals with a variety of controlled shapes. For example, we and other groups have demonstrated a simple and effective strategy for controlling the morphology of metal nanocrystals by introducing an oxidative etchant based on  $\text{Cl}^-/\text{O}_2$ ,<sup>[17–19]</sup>  $\text{Fe}^{\text{II}}/\text{Fe}^{\text{III}}$ ,<sup>[41]</sup> or  $\text{Cu}^{\text{I}}/\text{Cu}^{\text{II}}$  into the reaction solution.<sup>[42]</sup> Owing to the involvement of oxidative etching, any seed with twin defects will be preferentially oxidized back to the ionic form during a synthesis. As such, the proportions of single-crystal and twinned seeds can be altered in a control-

lable fashion to manipulate the shape taken by the nanocrystals. Most recently, corrosion was also demonstrated as a powerful method for transforming convex nanocrystals into concave nanocrystals through site-specific etching or galvanic replacement.

#### 3.1. Site-Specific Etching

The formation of a concave nanocrystal through site-specific etching relies on a localized dissolution process in which certain regions on the surface of a template are preferentially attacked by choosing a proper etchant. To this end, we have shown that such selective etching could be used to induce morphological evolution for Pd nanocrystals from solid nanocubes to nanocubes with pits on the surfaces and then nanocages with hollow interiors and porous walls. The key was to conduct the chemical synthesis in a mixture of ethylene glycol, water, and poly(vinyl pyrrolidone) (PVP), with  $\text{Na}_2[\text{PdCl}_4]$  serving as a precursor to elemental Pd.<sup>[26]</sup> The oxidative etching caused by  $\text{Cl}^-/\text{O}_2$  played a pivotal role in the initiation of pitting on the surface of the Pd nanocube. The presence of a small amount of water greatly enhanced the rate of oxidative etching. The PVP was also found to play a critical role in the formation of Pd nanocrystals with concave structures on the surfaces by passivating the surface to ensure a pitting mechanism.

In a recent study, Tilley and co-workers observed a morphological transition from cube to concave octapod with  $O_h$  symmetry, and then highly branched structures during the synthesis of Pt nanocrystals that involved the decomposition of  $\text{Pt}(\text{acac})_2$  under hydrogen in a mixture of toluene and



**Figure 1.** TEM images of Pt nanocrystals obtained at different stages of a synthesis, showing the formation of concave nanocubes and then branched structures owing to selective etching on the side faces and then edges of the nanocubes in conjunction with an overgrowth process: a) 75, b) 120, c) 240, and d) 500 min. (Modified with permission from Ref. [30], copyright 2009 American Chemical Society.)

oleylamine.<sup>[29,30]</sup> Figure 1 shows TEM images taken from products sampled at different stages of a synthesis, indicating that the different morphologies were formed by selective dissolution of Pt atoms from {100} facets in conjunction with the deposition of newly formed Pt atoms on {111} facets. Both etching and growth occurred simultaneously and at comparable rates. The Pt octapods with concave facets could be easily obtained by quenching the reaction at an appropriate stage. Interestingly, the selective etching was only observed in a synthesis conducted at a relatively high concentration of Pt(acac)<sub>3</sub>. As no halide ions were involved in this reaction, the authors believed that the etchant might have originated from acetylacetonate or a byproduct of acetylacetonate during the reaction. Based on the results of an earlier study reported by Masel and co-workers,<sup>[43]</sup> the authors suggested that an enol form of acetylacetone might act as a coordination ligand through chelation.

Noble-metal nanocrystals with concave surfaces have also been obtained by intentionally adding an appropriate etchant. To this end, Yang and co-workers reported an etching process for Ag octahedrons and were able to control the morphology of the resultant nanocrystals by manipulating the composition and/or concentration of the etchant.<sup>[20]</sup> For example, when subjected to an etchant consisting of NH<sub>4</sub>OH, H<sub>2</sub>O<sub>2</sub>, CrO<sub>3</sub>, and HCl, Ag octahedrons were successively transformed into truncated structures with pits at edges and then cubic hollow structures as the etchant was increased in concentration. This observation indicates a reversal of the reaction kinetics associated with the original overgrowth process, where {100}-bound cubes grew to become {111}-bound octahedrons with a ratio of 1.73 for the growth rates along the <100> and <111> directions. To selectively etch the corners and edges of the Ag octahedrons while keeping their {111} facets free from attack, a mixture of NH<sub>4</sub>OH and H<sub>2</sub>O<sub>2</sub> with a relatively weak etching power was employed as an etchant. Furthermore, localized etching at corners and edges was enhanced by using a highly concentrated etchant, resulting in concave structures

and eventually octapods with symmetry similar to the starting octahedrons. As the authors discussed, the key to obtaining Ag nanocrystals with a desirable concave morphology was to choose an etchant with an appropriate etching power: an etchant that is too strong may lead to isotropic etching, whereas an etchant that is too weak may not be able to attack the surface of a nanocrystal in the presence of capping agent(s).

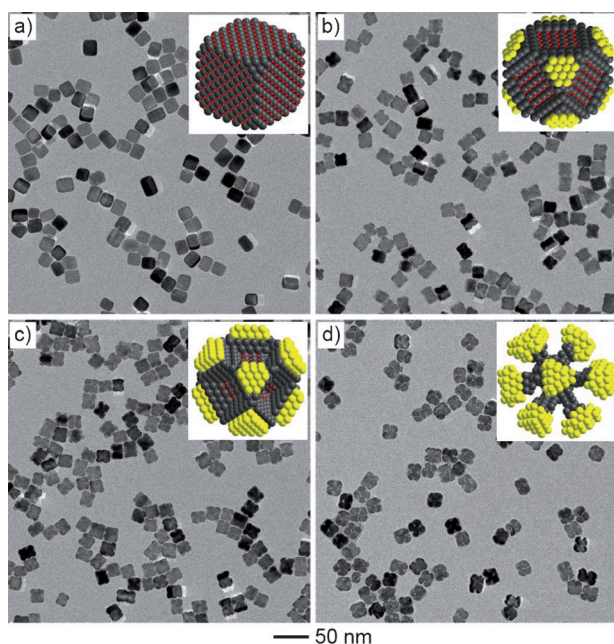
As a wet-chemistry approach, site-specific etching is well-suited for the production of concave nanocrystals in large quantities. The key to obtaining concave nanocrystals with the desired morphology is the selection of an etchant with the right anisotropy in reactivity and the use of sacrificial nanocrystals with matched facets on the surface. In general, the approach based on selective etching can be further extended to generate nanocrystals with concave surfaces and very complex morphologies.

### 3.2. Site-Specific Galvanic Replacement

As an approach based on corrosion, galvanic replacement represents a remarkably simple and versatile route to the synthesis of nanostructures with both hollow interiors and concave surfaces. Galvanic replacement is driven by the difference in electrochemical redox potential between a sacrificial template and the metal ions in a solution. The process can be described as the oxidation and dissolution of the template accompanied by the reduction of ions of a less-reactive metal and deposition of the resultant atoms on the surface of the template. The size and morphology of the final product can be varied by using sacrificial templates with different sizes and shapes or by controlling the extent of replacement.

As demonstrated in our early work, the galvanic replacement reaction could be exploited to prepare noble-metal nanoboxes and nanocages with tunable plasmonic properties.<sup>[44,45]</sup> For example, Au nanocages were generated by galvanic replacement between Ag nanocubes with truncated corners and H[AuCl<sub>4</sub>] in an aqueous solution.<sup>[44]</sup> The reaction started simultaneously from all corners of a truncated Ag nanocube, while the newly formed Au atoms were mainly deposited on the six side faces owing to the selective passivation of {100} facets by PVP. Concurrent with the deposition of Au, Ag was oxidized and removed from the interior to produce hollow and eventually porous structures (that is, nanocages) by alloying and dealloying. Continuous addition of H[AuCl<sub>4</sub>] eventually led to the formation of nanoframes, and finally fragmentation of the highly porous structures. Furthermore, Ag nanocrystals in other shapes, including nanocubes with sharp corners, nanospheres, nanorods, nanowires, and multiply twinned nanoparticles, have also been used with Au<sup>III</sup> or Au<sup>I</sup>, Pt<sup>IV</sup> or Pt<sup>II</sup>, and Pd<sup>II</sup> salt precursors to generate bimetallic nanostructures in the form of box, cage, frame, shell, rattle, and tube.<sup>[45]</sup> As this work on galvanic replacement has been thoroughly reviewed in several articles,<sup>[44,45]</sup> here we only concentrate on recent progress in galvanic replacement for the synthesis of noble-metal nanocrystals with concave surfaces.

In contrast to the formation of a Au nanocage through galvanic replacement that starts from the corners of a Ag nanocube, excavating a cube from the center of each side face will result in the formation of a concave nanocube. Most recently, we have demonstrated the synthesis of Pd-Pt nanocrystals with concave surfaces through galvanic replacement between Pd nanocubes and  $[\text{PtCl}_6]^{2-}$  in the presence of  $\text{Br}^-$ .<sup>[39]</sup> Products sampled at different reaction stages revealed a transition in morphology from nanocube to concave nanocube, and then octapod with enlarged bumps at the tips during the galvanic replacement (Figure 2). In this case, the Pd atoms



**Figure 2.** TEM images of Pd-Pt nanocrystals in the form of nanocubes, concave nanocubes, and octapods that were formed through  $\text{Br}^-$ -induced galvanic replacement at different reaction times: a) 0.5, b) 4, c) 9, and d) 20 h. (Modified with permission from Ref. [39], copyright 2011 American Chemical Society.)

on the {100} facets were preferentially oxidized and dissolved by reacting with  $\text{PtBr}_6^{2-}$  (a product of the reaction between  $\text{PtCl}_6^{2-}$  and  $\text{Br}^-$  due to ligand exchange). The resultant Pt atoms were subsequently deposited at the corner sites of a Pd nanocube. This observation was in contrast to what was observed in the galvanic replacement between Ag nanocubes with truncated corners and  $\text{H}[\text{AuCl}_4]$ .<sup>[44]</sup> As the galvanic reaction was continued, the Pd{100} facets were gradually removed together with the deposition of more Pt atoms at the corner sites, resulting in the formation of Pd-Pt concave nanocubes. The continuous deposition of newly formed Pt atoms at sites close to the corners of a Pd template eventually led to the formation of an octapod with a concave surface characterized by slightly elongated arms with enlarged bumps at the tips. By varying the amount of  $\text{H}_2[\text{PtCl}_6]$ , we could easily control the extent of galvanic replacement between Pd nanocubes and  $[\text{PtCl}_6]^{2-}$  ions to selectively obtain cubes with shallow pits on the side faces, concave cubes, and octapods.

The size and shape of the Pd-Pt concave nanocrystals could also be controlled by simply using Pd nanocrystals with different sizes and/or shapes as the templates.

From the viewpoint of electrochemical potential, the galvanic replacement between Pd and  $[\text{PtCl}_6]^{2-}$  should be able to occur spontaneously. However, no obvious sign of galvanic replacement between Pd nanocrystals and  $\text{H}_2[\text{PtCl}_6]$  was observed when they were mixed. We have shown that the addition of  $\text{Br}^-$  ions could promote the galvanic replacement between Pd nanocubes and  $[\text{PtCl}_6]^{2-}$  or more appropriately,  $[\text{PtBr}_6]^{2-}$ . The  $\text{Br}^-$ -induced replacement reaction showed high selectivity toward the Pd{100} facets, resulting in the formation Pd-Pt concave nanocubes and octapods. We believe that the preferential adsorption of  $\text{Br}^-$  ions on the Pd{100} facets and their strong coordination with  $\text{Pt}^{4+}$  ions are responsible for the localized, site-specific galvanic replacement.

#### 4. Concave Nanocrystals by Directionally Controlled Overgrowth

Seeded growth, in which newly formed atoms are added onto the surface of preformed seeds, offers a simple, versatile, and powerful approach to the synthesis of nanocrystals with controlled compositions and shapes. In general, the final products tend to take polyhedral shapes with convex surfaces, such as cuboctahedrons, cubes, octahedrons, icosahedrons, and decahedrons, depending on the number of twin defects in the seeds and the ratio of growth rates along  $\langle 111 \rangle$  and  $\langle 100 \rangle$  directions. Formation of a concave structure on the seed is not favored in terms of thermodynamics, which can be understood from the concept of chemical potential (defined as the Gibbs free energy per atom). The difference of chemical potential for an atom on a curved surface with respect to a flat surface is given by the Gibbs–Thomson equation:<sup>[46]</sup>

$$\Delta\mu = 2\gamma\frac{\Omega}{R} \quad (1)$$

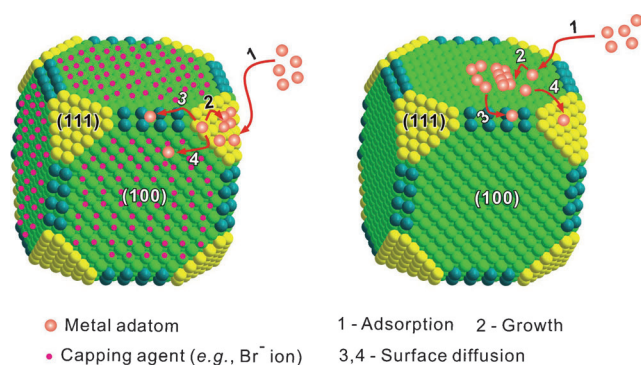
where  $\Delta\mu$  is the difference in chemical potential,  $\gamma$  is the surface tension,  $\Omega$  is the atomic volume, and  $R$  is the radius of curvature. From the viewpoint of geometry, a curved surface can be described by two principal radii of curvature,  $R_1$  and  $R_2$ . The chemical potential of an atom relative to a flat surface can therefore be expressed as:

$$\Delta\mu = 2\gamma\Omega\left(\frac{1}{R_1} + \frac{1}{R_2}\right) \quad (2)$$

For a concave surface, the radii of curvature ( $R_1$  and  $R_2$ ) are both negative, and the chemical potential of an atom on the concave surface is always lower than that on a flat surface. As such, the newly formed atoms should be preferentially added to the concave region during growth as driven by thermodynamics, leading to preferential overgrowth in this region and eventually elimination of the concave structure.

The limitation arising from thermodynamic confinement can be overcome by conducting the synthesis in the presence of a proper capping agent and/or under a kinetically-con-





**Figure 3.** Two different pathways for adding metal atoms to the surface of a growing cubic seed in the presence (left) and absence (right) of a capping agent.

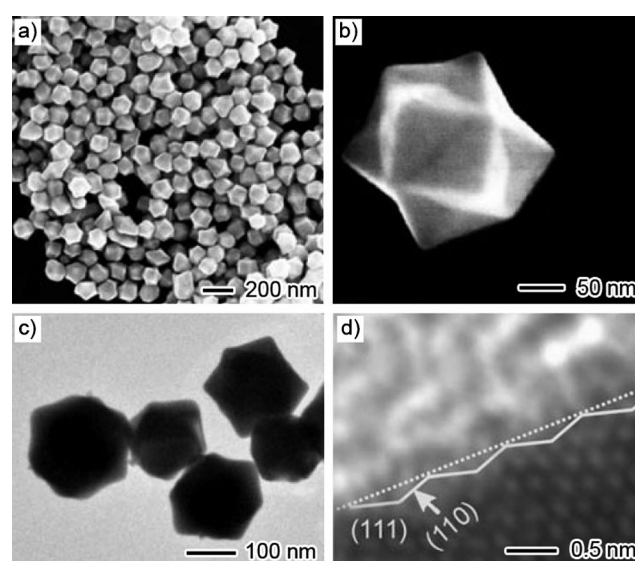
trolled mode (Figure 3). In these cases, it is no longer necessary to achieve the lowest total surface energy during seeded growth, resulting in the formation of a wide range of shapes deviated from the thermodynamically favored forms. In essence, a capping agent can selectively stabilize certain facets or low-coordination sites of a growing seed to promote the formation of various types of concave structures. As for kinetically-controlled growth, the newly formed atoms tend to be added to the edges and corners of a seed rather than the entire surface. As such, concave nanocrystals are expected to evolve from polyhedral seeds. In most cases, both mechanisms might be involved and it has been difficult to disentangle them.

#### 4.1. Facet-Selective Capping

A capping agent can selectively adsorb onto a specific type of facet on a growing seed and thus slow down the growth of this facet. Recent experimental studies show that a capping agent controls the shape of a noble-metal nanocrystal by changing the order of free energies associated with different crystallographic planes, and therefore their relative growth rates. For example, PVP can selectively passivate {100} rather than {111} facets of Ag to slow down their growth rate, resulting in the formation of a nanocube or a five-fold-twinned nanorod depending on the number of twin defects in the seed.<sup>[47]</sup> Halide ions, such as  $\text{Br}^-$  and  $\text{I}^-$ , have also been shown to selectively adsorb onto {100} instead of {111} facets, promoting the formation of cubes, bars, or rods mainly enclosed by {100} facets for noble metals including Ag, Pd, Pt, and Rh.<sup>[48–51]</sup> In contrast, citrate (either sodium citrate or citric acid) was found to bind more strongly to {111} than {100} facets of noble metals such as Ag and Pd, facilitating the formation of octahedrons, thin plates, decahedrons, or icosahedrons with a large portion of {111} facets on the surface.<sup>[52,53]</sup> In recent years, many other compounds have also been demonstrated as capping agents for controlling the shapes of noble-metal nanocrystals. For example, Zhang and co-workers reported the synthesis of Pd-Pt bimetallic tetrahedrons enclosed by {111} facets with oxalate ( $\text{C}_2\text{O}_4^{2-}$ ) serving as a capping agent for {111} facets.<sup>[54]</sup> Zheng and co-workers

demonstrated the synthesis of Pd nanosheets with {111} facets on the surface that were thinner than 10 atomic layers by using CO as a capping agent.<sup>[55]</sup> In some cases, the CO released from a precursor to the metal atom could also serve as a capping agent to promote the formation of Pt or Pd nanocrystals with surfaces dominated by {100} facets.<sup>[56–58]</sup> All these studies mainly concentrated on the synthesis of noble-metal nanocrystals with convex surfaces.

A capping agent can also be employed to direct the growth of noble-metal nanocrystals with concave structures on the surface by stabilizing low-coordination sites on the high-index facets. In this case, it is possible to generate novel concave nanocrystals, which are difficult to produce using kinetic control alone. For example, Xie and co-workers reported the synthesis of Au trisoctahedrons (TOHs) enclosed by high-index {221} facets at room temperature with cetyltrimethylammonium chloride (CTAC) as a capping agent (Figure 4).<sup>[22]</sup> A TOH can be considered as an octahe-



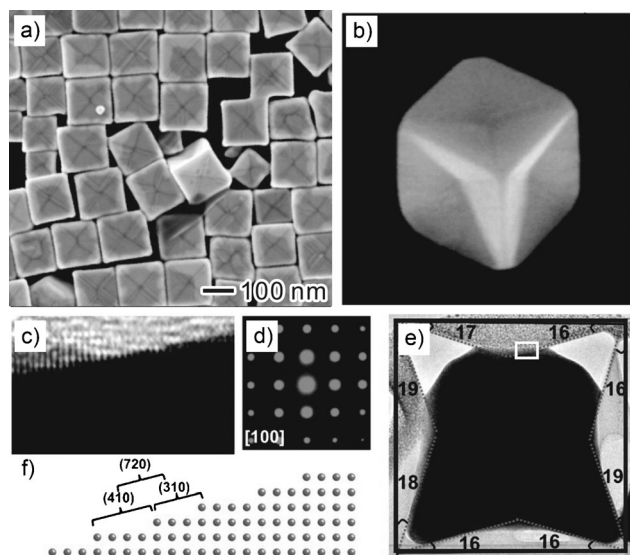
**Figure 4.** a, b) SEM, c) TEM, and d) HRTEM images of Au concave trisoctahedrons that were obtained through the reduction of  $\text{H}[\text{AuCl}_4]$  by ascorbic acid with CTAC as a capping agent at room temperature.<sup>[22]</sup>

dron whose eight triangular faces are pulled out to generate a sharp point.<sup>[59,60]</sup> Further studies revealed that the presence of CTAC played an important role in the formation of Au TOHs through selectively binding to low-coordination sites on the high-index facets.<sup>[23]</sup> In this case, it was suggested that the long alkyl ( $\text{CTA}^+$ ) chains had a size comparable to the atomic spacing on the high-index facets, making them more easily accommodated on less closely packed, high-index planes than the low-index planes, such as {100} and {111}. When a comparable amount of NaCl was introduced into the synthesis instead of CTAC, spherical nanocrystals of Au were obtained, indicating the capping role of  $\text{CTA}^+$  in the formation of Au TOHs. By replacing CTAC with cetyltrimethylammonium bromide (CTAB), however, Au nanocubes bounded by {100} facets dominated the final product. This change in morphology might arise from a competition

between  $\text{Br}^-$  and  $\text{CTA}^+$  for binding to the surface of Au nanocrystals. Combined together, both  $\text{CTA}^+$  and  $\text{Cl}^-$  ions are indispensable for the formation of Au TOHs. Furthermore, the precursor to Au atoms had to be reduced at an appropriate rate to maintain the TOH shape. A high reduction rate (as controlled by the concentration of reducing agent) could overshadow the differences between the growth rates of different facets, resulting in the formation of convex nanocrystals with a spherical shape.

The capping effect and facet selectivity are not limited to large surfactants and long-chain polymers; small molecules or inorganic ions may also have a profound impact on the growth rates along different crystallographic directions and thus the shape of nanocrystals owing to preferential binding. For example, a monolayer of Ag atoms could be preferentially deposited on specific facets of a Au nanocrystal by reducing  $\text{Ag}^+$  ions at a potential significantly less negative than that for bulk deposition through a mechanism widely known as underpotential deposition (UPD).<sup>[61]</sup> The Ag monolayer could selectively protect a specific type of facet of Au from further growth. As such, the preferential deposition of Ag can dramatically influence the growth rates of Au nanocrystals along different crystallographic directions and thus their shape and facets exposed on the surface. Furthermore,  $\text{Cl}^-$  ions were found to alter the UPD behavior of  $\text{Ag}^+$  ions on the surface of Au nanocrystals owing to the interaction between  $\text{Cl}^-$  and  $\text{Ag}^+$  ions.

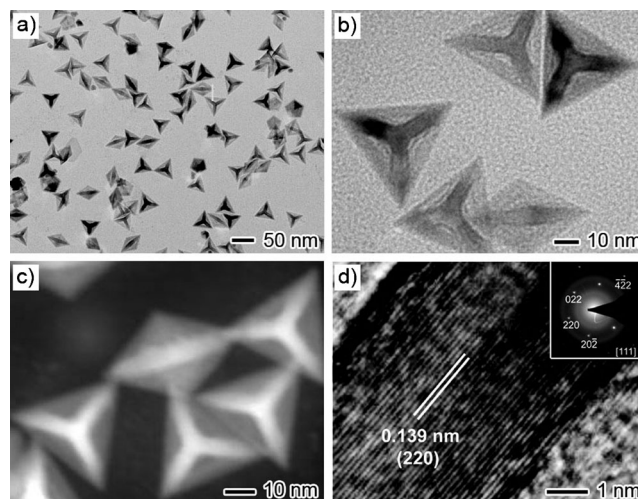
Using a combination of  $\text{Ag}^+$  and  $\text{Cl}^-$  ions, Mirkin and co-workers reported the synthesis of Au concave nanocubes enclosed by 24 high-index {720} facets through a seed-mediated synthetic method (Figure 5).<sup>[24]</sup> The size of the Au concave nanocubes could be easily adjusted from tens to hundreds of nanometers by varying the amount of Au seeds



**Figure 5.** a,b) SEM images of Au concave nanocubes, c) HRTEM image of the edge of a high-index facet, d) electron diffraction pattern of the sectioned concave cube, e) zoomed-in image of a single cut concave cube aligned edge-on, and f) atomic model of the {720} facet, projected from the [001] direction, corresponding to the region indicated with a box in (e). (Modified with permission from Ref. [24], copyright 2010 American Chemical Society.)

added to the reaction solution. In contrast to the synthesis of Au TOHs,<sup>[23]</sup> a monolayer of Ag atoms deposited on the surface of Au seeds by UPD was believed to be responsible for the formation of concave nanocubes of Au. By replacing CTAC with CTAB and keeping other conditions unchanged, Au tetrahexahedrons (THHs) enclosed by 24 high-index {037} facets instead of concave nanocubes were obtained.<sup>[62]</sup> The different binding affinity of  $\text{Cl}^-$  and  $\text{Br}^-$  to a Au surface was thought to be responsible for the morphological transition from concave cubes to THHs. Although the exact mechanism is yet to be resolved, the ionic species including metal and halide ions offer an effective means for controlling the exposed facets and surface curvature of Au nanocrystals.

The approach based on the facet-selective capping effect of ionic species has also been extended to other noble metals, such as Pd and Pt. The key is to select an appropriate capping agent or ionic species for the specific metal. For example, Zheng and co-workers reported the synthesis of tetrahedral and trigonal bipyramidal nanocrystals of Pd with concave structures on the surface using a solvothermal process in the presence of formaldehyde.<sup>[27]</sup> As shown in Figure 6, the concave tetrahedron can be considered as an excavated



**Figure 6.** Morphological and structural characterizations of Pd concave tetrahedrons that were obtained using a solvothermal approach in the presence of formaldehyde. a,b) TEM images, c) HAADF-STEM, and d) HRTEM image. Inset: selected electron diffraction pattern. (Modified with permission from Ref. [27], copyright 2009 American Chemical Society.)

tetrahedron with a trigonal pyramid excavated at the center of each face, with the surface mainly enclosed by {110} facets. This concave structure was a result of fast growth along a combination of  $\langle 100 \rangle$  and  $\langle 110 \rangle$  directions of a tetrahedral seed. When formaldehyde was substituted with other aldehydes, such as benzaldehyde, similar concave structures were also formed, indicating that the aldehyde group played an important role in the formation of concave structures. Specifically, the aldehyde group was supposed to dramatically retard the growth rate of a Pd seed along  $\langle 111 \rangle$  directions by selectively capping the {111} facets and thus promoting the

formation of concave tetrahedrons. This mechanism was supported by the successful synthesis of Pd octahedrons seeded by Pd cubes, with formaldehyde serving as both reducing and capping agents.<sup>[63]</sup> In another example, Zheng and co-workers have demonstrated the solvothermal synthesis of Pt concave nanocrystals with high-index {411} facets and a unique octapod morphology by introducing methylamine as a capping agent.<sup>[31]</sup> The Pt concave octapods were believed to form through preferential growth along  $\langle 111 \rangle$  directions at the corners of a cubic seed. The authors suggested that the preferential binding of amine group to the {100} facets of Pt nanocrystals was responsible for the directional overgrowth and thus the formation of concave structures. The high-index {411} facets were preserved during the synthesis because the amine group could bind to and stabilize the low-coordination Pt sites.

Overall, the use of a capping agent is an effective approach to shape-controlled synthesis of noble-metal nanocrystals with concave structures on the surface. Furthermore, the capping agent could be potentially used to control the exposed facets by manipulating the ratio of growth rates along different crystallographic directions. However, the approach based on a capping agent is not generic, because the same capping agent can bind differently to the surfaces of different noble metals. As such, it is still very difficult to rationally identify or design a capping agent to direct the growth of noble metals into nanocrystals with specific facets. In some cases, the effect of a capping agent can also be understood in terms of kinetic control rather than surface binding because the capping agent can form complexes with metal ions to alter the reduction kinetics (see the next section). To address these issues, the binding affinity of a capping agent for the surface of a metal nanocrystal or the metal ions should be understood first at the atomic level through a combination of theoretical simulations and various surface characterization techniques.<sup>[64,65]</sup>

#### 4.2. Kinetically Controlled Overgrowth

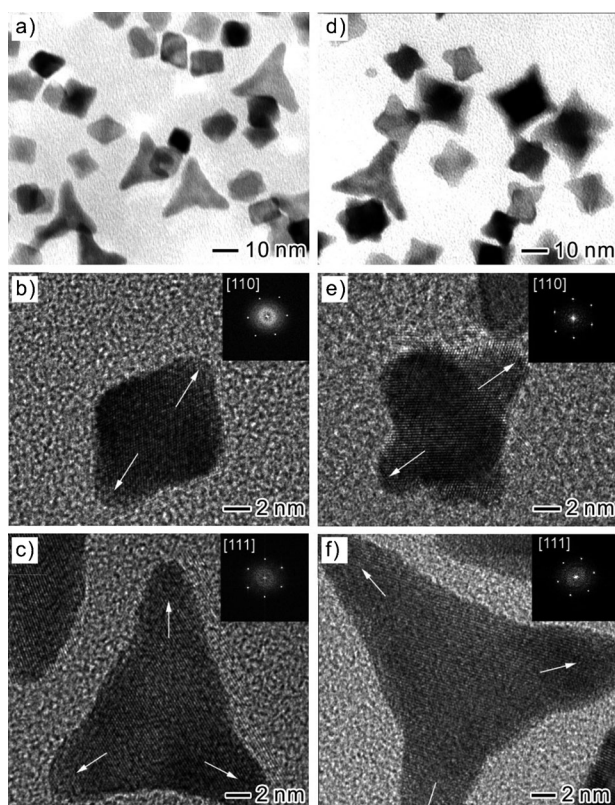
Over the past decade, kinetic control has emerged as a versatile and powerful approach to shape-controlled synthesis of noble-metal nanocrystals in the solution phase. As an important feature, the products obtained under kinetic control are not limited by thermodynamic confinement, allowing for the formation of nanocrystals with concave surfaces. A kinetic control is based on manipulation of the growth rate at which atoms are generated and added to the surface of a seed. Depending on the presence or absence of a capping agent, atoms generated from a precursor can be added to the surface of a growing seed in two different ways (Figure 3), leading to nanocrystals with different morphologies. For a cubic seed, when the six side faces are strongly passivated by a capping agent (such as  $\text{Br}^-$  for Pd), the newly formed atoms are expected to nucleate and grow from the corner sites. In contrast, the atoms will be preferentially added to the side faces of a cubic seed in the absence of a capping agent (or when the supply of capping agent becomes insufficient during growth) owing to a much larger

surface area for the side faces relative to the corners. In the following steps, the adsorbed atoms could also migrate to other regions on the seed including corners, edges, and side faces, owing to the involvement of surface diffusion.<sup>[66]</sup>

The probability that an adsorbed atom will stay or migrate to a different site is largely determined by the rate at which the atom is produced, and thus the experimental conditions related to reaction kinetics. For example, at a high rate of conversion from precursor to atom together with strong capping of the side faces, the probability for the atoms to migrate from corner sites to side faces is rather low, and growth is expected to largely occur along the  $\langle 111 \rangle$  directions. When the atoms are supplied at a significantly reduced rate, they will have enough time to migrate to other sites such as edges and even side faces after they have been deposited on the corners of a cubic seed. In these cases, concave and conventional cubes will be obtained depending on how strongly the capping agent binds to and thus passivates the atoms on side faces. In the absence of a capping agent, atoms generated from precursor at a high rate will stay to grow on the side faces of a cubic seed, resulting in the formation of a concave octahedron. When the kinetics are slowed down, a large portion of the adsorbed atoms on the side faces of a cubic seed will have enough time to migrate to corners and edges, leading to the formation of conventional octahedrons. As a result, the migration of atoms on the surface of a growing seed through surface diffusion together with the effect of a capping agent will play the most significant role in determining the growth habit of a seed, and thus the shape or morphology taken by the final product.

In general, the reaction kinetics involved in a synthesis of noble-metal nanocrystals can be manipulated by adjusting many different experimental parameters, including variations of the types of precursor and reductant, their concentrations, their injection rates, the reaction temperature, and the introduction of coordination ligands for the metal ions. For example, we have demonstrated the synthesis of Pt tetrapods and hexapods with concave structures on the surface by adding ionic species, such as  $\text{NO}_3^-$ , into a conventional polyol synthesis (Figure 7).<sup>[32]</sup> As the concentration of  $\text{NO}_3^-$  was increased, the morphology of Pt nanocrystals evolved from nanoparticles with a rounded profile to tetrapods and hexapods with concave surfaces due to kinetically-controlled overgrowth. The extent to which the surface is concave (determined by curvature radius) was sensitive to the molar ratio of  $\text{NO}_3^-$  to  $\text{PtCl}_6^{2-}$  (Figure 7a–c and d–f, where the ratios were 5.5 and 11, respectively). In this approach, nitrite ( $\text{NO}_2^-$ ) ions resulting from the reduction of nitrate ( $\text{NO}_3^-$ ) by  $\text{PtCl}_4^{2-}$  could form stable complexes with both  $\text{Pt}^{\text{II}}$  and  $\text{Pt}^{\text{IV}}$  species, and thus greatly slow down the rate at which Pt atoms were produced from the reduction of Pt precursor by ethylene glycol (EG). This mechanism was consistent with the UV/Vis spectra taken at different time points during the synthesis. As only PVP was involved as a stabilizing agent, the formation of Pt atoms at a slow rate allowed for surface migration of the newly adsorbed Pt atoms from side faces to corners on a growing Pt seed owing to higher reactivity for the corner sites. As a result, concave nanocrystals of Pt were ultimately formed through preferential overgrowth at the corner sites of

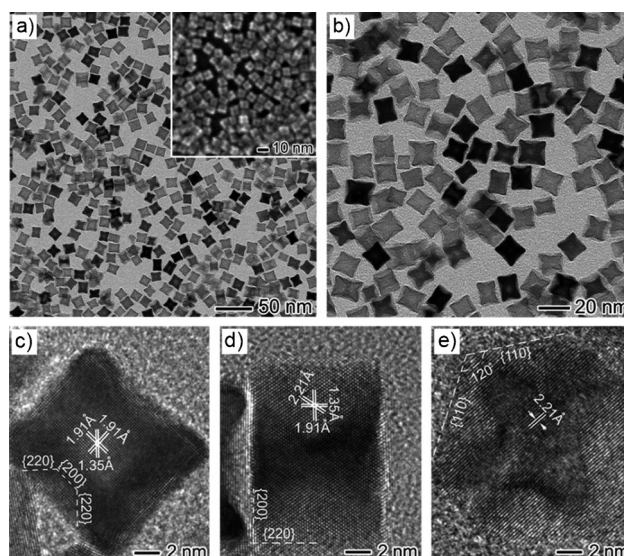




**Figure 7.** TEM and HRTEM images of Pt nanocrystals that were obtained with the molar ratio of  $\text{NaNO}_3$  to  $\text{H}_2[\text{PtCl}_6]$  being controlled at a–c) 5.5 and d–f) 11.0, respectively. Insets: corresponding Fourier transform patterns. (Modified with permission from Ref. [32], copyright 2004 American Chemical Society.)

both tetrahedral and octahedral Pt seeds, which were, in turn, formed at the beginning of a synthesis through homogeneous nucleation.

Using a similar strategy, we recently demonstrated a polyol process for shape-controlled synthesis of Rh nanocrystals with concave surfaces by manipulating the reaction kinetics with a syringe pump to alter the injection rate of a salt precursor.<sup>[34]</sup> By injecting the precursor into a reaction solution at a slow rate ( $4 \text{ mL h}^{-1}$ ), a large number of Rh concave nanocubes with an average edge length of 15 nm were obtained. Figure 8 shows morphological and structural characterizations, suggesting that each concave Rh nanocube was composed of six square  $\{100\}$  faces with a small area, six square  $\{100\}$  faces with a large area but with a square hole in the center, and 24 isosceles trapezium-like  $\{110\}$  side faces. This structure could be visualized as a concave cube with a truncated square pyramid excavated at the center of each face. Analyses of the samples obtained at different reaction times suggest that the Rh concave nanocubes were formed through preferential overgrowth at both the corner and edge sites of a cubic seed along the  $\langle 111 \rangle$  and  $\langle 110 \rangle$  directions, respectively. In comparison, a faster injection rate (for example,  $60 \text{ mL h}^{-1}$ ) resulted in the formation of concave octapods by accelerated overgrowth only at the corner sites of a cubic seed along the  $\langle 111 \rangle$  direction. Combined together, it is clear that kinetically controlled overgrowth could generate

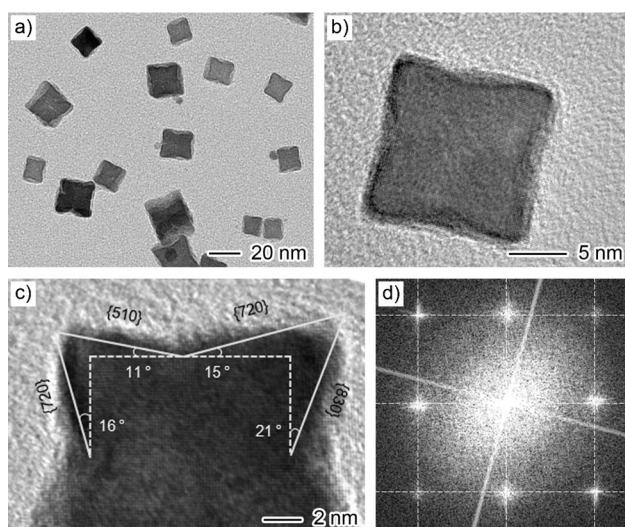


**Figure 8.** Morphological and structural characterizations of a typical sample of Rh concave nanocubes prepared at  $140^\circ\text{C}$  with an injection rate of  $4 \text{ mL h}^{-1}$ . a,b) TEM images of the as-prepared sample, and c–e) HRTEM images of individual concave nanocubes recorded along the  $[100]$ ,  $[110]$ , and  $[111]$  zone axes. The inset in (a) shows a typical SEM image of the concave nanocubes. (Modified with permission from Ref. [34], copyright 2011 American Chemical Society.)

many different types of concave structures depending on the sites or directions of preferential growth.

The surface diffusion of Rh atoms on cubic seeds was believed to be responsible for the formation of Rh nanocrystals with different shapes observed at different injection rates for the precursor. In the initial stages, Rh atoms generated from the injected precursor were expected to preferentially diffuse to the most active sites (eight corners) of a cubic seed owing to the selective adsorption of  $\text{Br}^-$  on the  $\{100\}$  side faces.<sup>[67]</sup> Thereafter, the Rh atoms at corners would stay and grow along the  $\langle 111 \rangle$  directions or migrate to other sites, such as edges and side faces, by surface diffusion. The ratio of atoms associated with these two types of growth modes should be mainly determined by the concentration of Rh atoms and thus the injection rate for the precursor. As the  $\{100\}$  facets were strongly blocked by  $\text{Br}^-$  ions, the Rh atoms could only migrate from corners to edges on a cubic seed. When the injection rate was slow, it would take a relatively long time to achieve a high level of supersaturation around the corners of a cubic seed. During this period, most of the Rh atoms at corners should have enough time to migrate to edges through surface diffusion. As a result, the cubic seed would grow at both corners and edges along the  $\langle 111 \rangle$  and  $\langle 110 \rangle$  directions, respectively, at a more or less similar rate. In contrast, the Rh atoms around corners were always retained at a high supersaturation when a fast inject rate was involved. As a result, growth along the  $\langle 111 \rangle$  directions was accelerated relative to the  $\langle 110 \rangle$  directions as only a small number of Rh atoms could have enough time to migrate to the edges. As the growth occurred preferentially at the corners along  $\langle 111 \rangle$  directions, the product eventually evolved into an octapod.

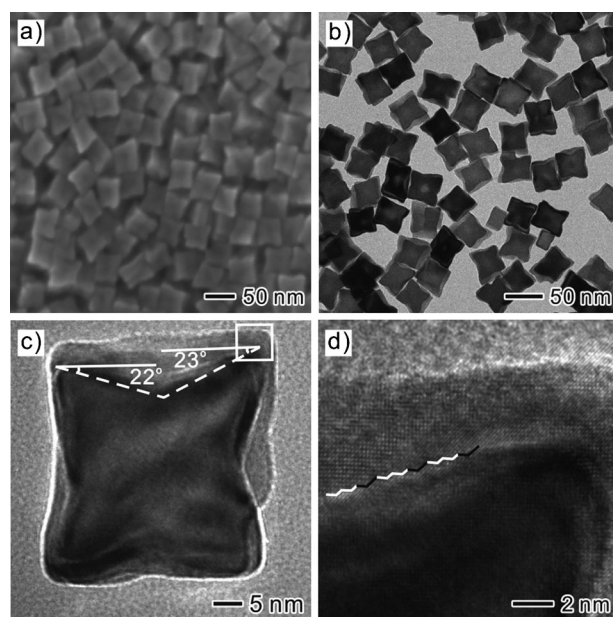
The kinetically controlled strategy has also been successfully extended to syntheses of other noble metals with



**Figure 9.** Morphological and structural characterizations of a typical sample of Pt concave nanocubes synthesized by continuously adding an aqueous  $\text{NaBH}_4$  solution and a mixture of  $\text{K}_2[\text{PtCl}_4]$ ,  $\text{KBr}$ , and  $\text{Na}_2\text{H}_2\text{P}_2\text{O}_7$  using two syringe pumps into water held at  $95^\circ\text{C}$ . The injection rate was  $67\ \mu\text{L min}^{-1}$ , and the ratio of  $\text{KBr}$  to  $\text{Na}_2\text{H}_2\text{P}_2\text{O}_7$  was 3:1. a,b) TEM images, c) HRTEM image recorded along the  $[001]$  zone axis, and d) Fourier transform pattern of the concave nanocube.<sup>[33]</sup>

a concave structure in a water-based solution. For example, we recently demonstrated the synthesis of Pt nanocubes with a concave structure on the surface by slowly adding a  $\text{NaBH}_4$  solution and a mixture containing  $\text{K}_2[\text{PtCl}_4]$ ,  $\text{KBr}$ , and  $\text{Na}_2\text{H}_2\text{P}_2\text{O}_7$  into deionized water held at  $95^\circ\text{C}$  using two syringe pumps.<sup>[33]</sup> As shown in Figure 9, a large number of Pt concave nanocubes with an average size of 15–40 nm were generated by reduction of the Pt precursor by  $\text{NaBH}_4$ . The surface of the Pt concave nanocube was mainly enclosed by  $\{720\}$ , together with some other high-index facets, such as  $\{510\}$ ,  $\{830\}$ , and  $\{310\}$ . The key to the success of this method was the formation of Pt-pyrophosphato complex between  $\text{Na}_2\text{H}_2\text{P}_2\text{O}_7$  and  $\text{K}_2[\text{PtCl}_4]$ , and manipulation of the reaction kinetics using a syringe pump as well as the use of  $\text{Br}^-$  ions both as capping and complexing agents. After mixing of  $\text{K}_2[\text{PtCl}_4]$  and  $\text{Na}_2\text{H}_2\text{P}_2\text{O}_7$ , the Pt pyrophosphato complex quickly formed as a new precursor to Pt atoms, with the reduction rate being greatly retarded. The amount of  $\text{KBr}$  also had a great influence on the reduction kinetics involved in the reaction. A high concentration of  $\text{KBr}$  was found to further slow down the reduction rate of Pt precursor by increasing the amount of  $[\text{PtBr}_4]^{2-}$ , which has a much larger stability constant relative to  $[\text{PtCl}_4]^{2-}$ .<sup>[68]</sup> As a result, Pt nanocubes with a concave structure were formed owing to the strong capping of  $\{100\}$  facets by  $\text{Br}^-$  ions and the surface migration of Pt atoms from corners to edges.

During the formation of concave nanocrystals, the concentration of reactant also plays an important role in controlling the reaction kinetics and thus the growth habit. Recently, we synthesized Pd concave nanocubes (Figure 10) by starting with Pd nanocubes as the seeds and manipulating the concentrations of reactants, including  $\text{Na}_2[\text{PdCl}_4]$ ,  $\text{KBr}$ , and ascorbic acid.<sup>[28]</sup> Our morphological and structural

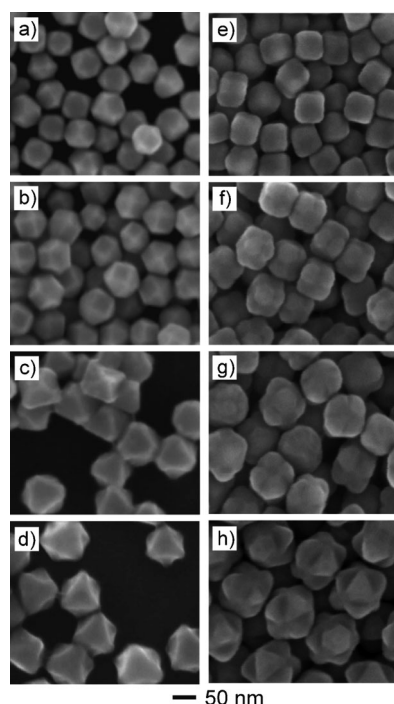


**Figure 10.** Morphological and structural characterizations of a typical sample of Pd concave nanocubes synthesized by manipulating the concentrations of reactants including  $\text{Na}_2[\text{PdCl}_4]$ ,  $\text{KBr}$ , and ascorbic acid, with Pd cubes serving as the seeds. a) SEM, b) TEM, and c,d) HRTEM images.<sup>[28]</sup>

characterizations confirmed the formation of Pd concave nanocubes enclosed by 24 high-index  $\{730\}$  facets. The sizes of these concave nanocubes could be controlled in the range of 15–35 nm by simply using Pd nanocubes with different edge lengths as the seeds. We found that a low concentration of  $\text{Na}_2[\text{PdCl}_4]$  was beneficial to the formation of Pd concave nanocubes by preferential overgrowth at corner and edge sites of a cubic seed. Obviously, the slow supply of Pd atoms at a relatively low concentration of  $\text{Na}_2[\text{PdCl}_4]$  dramatically reduced the probability of surface migration from corners to side faces when  $\text{Br}^-$  was used as a capping agent to block the  $\{100\}$  facets. These conditions facilitated selective overgrowth of cubic seeds from corners and edges along  $\langle 111 \rangle$  and  $\langle 110 \rangle$  directions and thus the formation of Pd nanocubes with concave surfaces. Furthermore, a low concentration of  $\text{KBr}$  and a high concentration of ascorbic acid were also found to promote the selective overgrowth at corners and edges of a cubic seed and thus the formation of concave nanocubes. In these two cases, the migration of Pd atoms from corners to side faces of a cubic seed was greatly inhibited by increasing the generation rate of Pd atoms with  $\text{Br}^-$  serving as a capping agent to block the  $\{100\}$  face.

We have also demonstrated the synthesis of Au hexapods with concave surfaces and arms of different lengths by using Au octahedrons as the seeds and manipulating the concentration of the precursor ( $\text{H}[\text{AuCl}_4]$ ).<sup>[25]</sup> The formation of Au hexapods was attributed to the preferential overgrowth at six vertices of each octahedral seed (the most active site) along the  $\langle 100 \rangle$  direction. Most recently, we have also showed a facile approach to the synthesis of Ag concave nanocrystals by seed-mediated growth (Figure 11).<sup>[21]</sup> The synthesis involved the use of Ag nanocubes as seeds in an aqueous





**Figure 11.** SEM images showing the evolution of: a–d) Ag concave octahedrons and e–h) Ag concave trisoctahedrons through a seed-mediated overgrowth.<sup>[21]</sup> The volume of  $\text{AgNO}_3$  injected was a) 0.8, b) 2, c) 4, d) 5; e) 1.5, f) 3.5, g) 6.5, and h) 10 mL.

system, with L-ascorbic acid serving as a reductant and  $\text{AgNO}_3$  as a salt precursor. In the absence of a strong capping agent, we found that increasing the concentration of ascorbic acid accelerated the deposition rate of Ag atoms on the side faces of a cubic seed along the  $\langle 100 \rangle$  directions, resulting in the formation of an octahedron with a concave structure on each one of its side faces. When  $\text{Cu}^{2+}$  ions were introduced, however, the dominance of growth was switched to the  $\langle 111 \rangle$  directions, forcing the cubic seed to sequentially evolve into a concave cube, an octapod, and finally a concave trisoctahedron, with all of them being enclosed by high-index facets. We believe that the surface migration of Ag atoms on a growing seed as well as the surface capping of  $\text{Cu}^{2+}$  were responsible for the formation of these new types of Ag concave nanocrystals. In the absence of  $\text{Cu}^{2+}$ , most of the Ag atoms generated from the reduction of  $\text{AgNO}_3$  were initially added to the side faces of a cubic seed. The high supply rate for Ag atoms associated with the increase of ascorbic acid concentration facilitated the deposition of Ag atoms on the side faces of a cubic seed along the  $\langle 100 \rangle$  directions, and thus the formation of Ag octahedrons with concave surfaces. In contrast, the introduction of a large number of  $\text{Cu}^{2+}$  prompted surface diffusion for the freshly generated Ag atoms in the initial stages owing to the capping effect of  $\text{Cu}^{2+}$  for Ag  $\{100\}$  facets. In this case, the surface migration of Ag atoms only took place from corners to edges of a cubic seed, resulting in the morphology evolution from a cube to a concave cube, an octapod, and finally a concave trisoctahedron.

The kinetically controlled approach to concave nanocrystals has also been applied to bimetallic systems. For

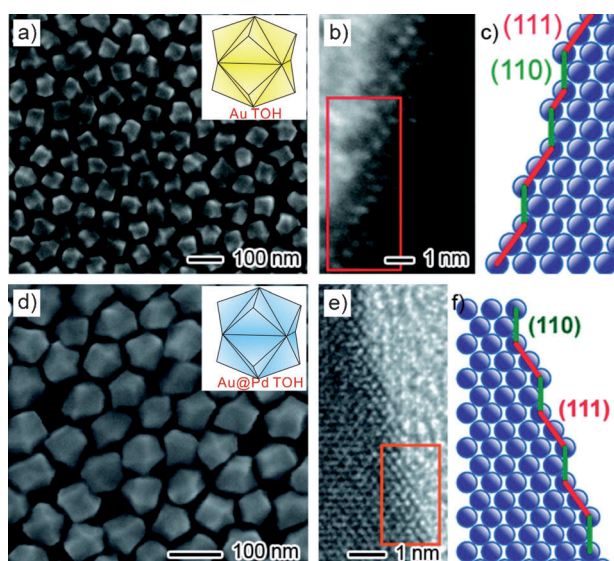
example, we prepared Pt–Rh concave nanocubes using a procedure similar to what was used for the synthesis of Rh concave nanocubes, except for the use of Pt cubes as the seeds.<sup>[34]</sup> Huang and co-workers used Au nanocubes as seeds to generate Au–Pd core-shell nanocrystals with different shapes using CTAC as a capping agent.<sup>[35]</sup> The reaction temperature was found to play an important role in determining the exact shape or morphology. A low temperature (for example,  $10^\circ\text{C}$ ) facilitated the formation of Au–Pd concave octahedrons, while Au–Pd nanocrystals with a THH shape were obtained when the reaction temperature was increased to  $30\text{--}60^\circ\text{C}$ . As the authors suggested, the growth rates at corners and edges of an octahedron along the  $\langle 100 \rangle$  and  $\langle 110 \rangle$  directions, respectively, might be substantially faster than that at faces along the  $\langle 111 \rangle$  direction at low temperature, leading to the formation of the concave octahedron. Recently, Skrabalak and co-workers demonstrated the synthesis of Au–Pd concave octapods and octahedrons by coupling seed-mediated synthesis with co-reduction of  $\text{H}[\text{AuCl}_4]$  and  $\text{H}_2[\text{PdCl}_4]$ .<sup>[36]</sup> By increasing the amount of  $\text{H}_2[\text{PdCl}_4]$ , the morphology of the Au–Pd nanocrystals evolved from concave octapods to concave octahedrons, which could be attributed to the difference in growth rate caused by the pH-dependent reduction power of ascorbic acid. A similar synthesis was also reported by Han and co-workers.<sup>[69]</sup> Most recently, Xie and co-workers also reported a facile co-reduction method for the synthesis of hexoctahedral Au/Pd alloy nanocrystals with concave structures on the surface in the presence of octadecyltrimethyl ammonium chloride (OTAC) and  $\text{Cu}^{2+}$  ions.<sup>[70]</sup> The Au/Pd alloy hexoctahedra enclosed by 48 high-index  $\{431\}$  facets was evolved from a tetrahedron by pushing the center of every square edge toward the center. Again, the UPD of Cu and the capping effect of OTAC were found to play important roles in generating the hexoctahedral Au/Pd alloy nanocrystals. For a heterogeneous system, however, other issues such as lattice mismatch and bonding energy between the core and shell metals should also be considered.<sup>[71,72]</sup> Still, there is a strong interest in further developing the synthesis of concave nanocrystals with different elemental compositions using kinetically controlled overgrowth.

As illustrated by the aforementioned samples, kinetic control is a powerful route to concave nanocrystals with unusual facets and negative curvature from noble metals, such as Ag, Au, Pt, Rh, and Pd, as well as a combination of them. The migration of atoms on the surface of a growing seed through surface diffusion as well as surface capping were found to play a pivotal role in determining the growth habit of a noble-metal nanocrystal, and thus its final shape or morphology. Experimentally, kinetic control can be achieved by manipulating an array of parameters, including the reagent concentration, the injection rate, the temperature, the addition of ionic species, or a combination of them. The combination of kinetic control and manipulation of growth rate along different crystallographic directions through the use of a capping agent is expected to emerge as the most versatile approach to synthesis of concave nanocrystals with well-controlled facets on the surface.



### 4.3. Template-Directed Epitaxy

Template-directed epitaxy provides a straightforward and effective route to nanocrystals with well-controlled facets. When used for the synthesis of concave nanocrystals, templates with concave surfaces were initially prepared using one of the methods discussed above, and then combined with the epitaxial deposition of a different metal. In this case, the concave morphology and the type of facet on the surface can both be retained while the outermost layer is being switched from one metal to another. To this end, Wang and co-workers reported the epitaxy of Pd on Au TOHs with both concave surfaces and high-index facets.<sup>[37]</sup> The Au TOHs enclosed by 24 high-index {221} facets (Figure 12a,b) were in turn prepared by reducing H[AuCl<sub>4</sub>] in an aqueous CTAC



**Figure 12.** Morphological and structural characterizations of a–c) Au and d–f) Au-Pd trisioctahedral (TOH) nanocrystals. a,d) SEM image, b,e) HRTEM images taken from edges to show the high-index facets, and c,f) two-dimensional lattice model illustrating the high-index (221) facet. The insets in (a) and (d) illustrate the Au and Au-Pd TOH nanocrystals. (Modified with permission from Ref. [37], copyright 2011 American Chemical Society.)

solution with ascorbic acid as a reducing agent in the presence of Au seeds.<sup>[22]</sup> During epitaxy, the concave structures on the Au trisioctahedron were faithfully transferred into the Pd shell when its thickness was controlled within a few nanometers. The final products were concave Au@Pd TOHs, with Au in the core and Pd in the shell (Figure 12c,d). The amount of Pd precursor (Na<sub>2</sub>PdCl<sub>4</sub> in this case) played an important role in the successful synthesis of Au@Pd core-shell TOHs. Increasing the amount of Na<sub>2</sub>PdCl<sub>4</sub> to a certain level resulted in disappearance of the concave structures owing to an intrinsically higher growth rate in these regions than the convex regions.

Along with the templating effect, the reaction kinetics involved in epitaxial deposition of the shell was also critical to the formation of concave products. In a recent study, Lee and co-workers demonstrated a kinetically-controlled synthesis of

Au@Pd concave nanocrystals enclosed by adjustable, high-index Pd facets with Au TOHs as the templates by controlling the atomic ratio of Pd to Au and using different amounts of NaBr.<sup>[38]</sup> Increasing the atomic ratio of Pd to Au resulted in the formation of Au@Pd core-shell nanocrystals with a morphological transition from concave TOH encased by high-index {552} facets to concave hexoctahedron enclosed by high-index {432} facets owing to faster growth along the  $\langle 110 \rangle$  direction. The addition of NaBr further promoted the preferential growth of Pd along the  $\langle 110 \rangle$  direction owing to selective adsorption of Br<sup>−</sup> on the {100} facets. The nanocrystals evolved into concave Au@Pd THHs with different types of high-index facets on the surface, depending on the amount of NaBr added.

Template-directed epitaxy is a simple and versatile route to concave nanocrystals with various types of high-index facets. As a prerequisite, the templates must be produced in high quality and relatively large quantities. For the epitaxial deposition, some specific rules have to be observed to ensure a successful synthesis of concave nanocrystals with a core-shell structure.<sup>[71]</sup> For example, the lattice mismatch between the two metals must be kept below 5 %, as large mismatches tend to prevent the layered, epitaxial overgrowth of a second metal on the concave template. The electronegativity of the second metal should be smaller than that of the template metal to avoid the potential involvement of galvanic replacement. Moreover, the bond dissociation energy between the shell atoms should be smaller than that between the core and shell atoms. In regard to these points, both Pt and Rh are good choices of template materials for the synthesis of concave nanocrystals made of other noble metals, including Ag, Pd, and Au.

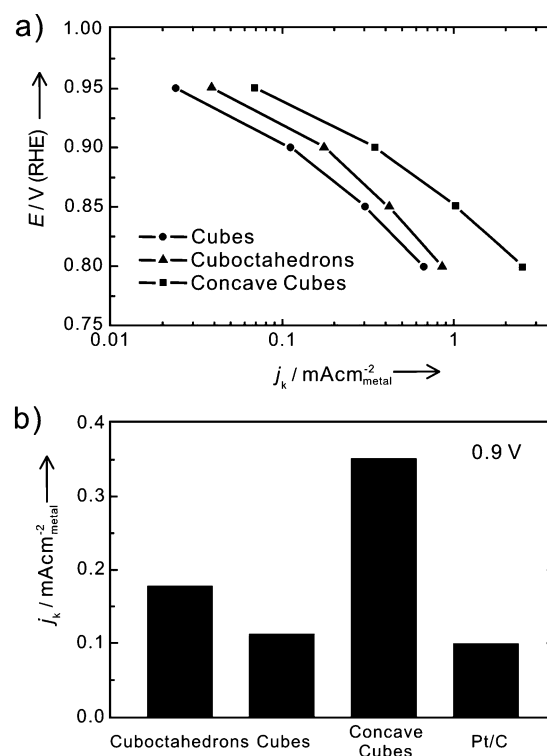
### 5. Catalytic Properties and Related Applications

Noble metals enjoy widespread use as catalysts for a wide variety of industrially relevant chemical reactions. For example, Pt is a primary component of the catalysts used in three-way automotive catalytic conversion, petroleum refining, production of nitric acid, and fuel-cell technology.<sup>[73,74]</sup> Palladium is also a critical component of the catalysts currently utilized for low-temperature reduction of automobile pollutants, as well as hydrogenation reactions, CO oxidation, and organic reactions such as Suzuki or Heck coupling.<sup>[75,76]</sup> To maximize their performance in these applications, a great deal of effort has been devoted to the development of catalysts with superior activity/selectivity by controlling the size, shape, and composition. Noble-metal nanocrystals with concave structures on the surface are of particular importance to catalysis because of their exposed high-index facets and thus high densities of atomic steps, edges, and kinks, which can all contribute as highly active sites for breaking chemical bonds. For example, Zheng and co-workers recently reported the catalytic properties of Pt concave nanocrystals with 24 high-index {441} facets (prepared using a solvothermal process in the presence of methylamine; see Section 4.1) for electrocatalytic oxidation of formic acid.<sup>[31]</sup> The specific activity of these concave

nanocrystals in terms of equivalent electrochemically active surface area (ECSA) was 2.3 and 5.6 times greater than those of commercial Pt black and Pt/C, respectively, owing to the presence of active sites with low coordination numbers.

Suzuki coupling is one of the most powerful and versatile methods in organic chemistry for the formation of biaryls, polyolefins, styrenes, and biphenyls.<sup>[76]</sup> This reaction can serve as a model system to test the catalytic performance of Pd nanocrystals with different shapes or facets. In a recent study, we investigated the catalytic properties of Pd concave nanocubes with high-index {730} facets (prepared using a kinetically-controlled method; see Section 4.2) for the formation of biphenyl through Suzuki coupling between phenylboronic acid and iodobenzene.<sup>[28]</sup> For Pd concave nanocubes of 37 nm in size, 99% of iodobenzene was converted into biphenyl after 20 min. In comparison, a conversion of only 38% was achieved when the conventional Pd nanocubes with a similar size were used as a catalyst under the same conditions. The intrinsic turnover frequency (TOF, defined as the conversion of iodobenzene per surface Pd atom per second) of Pd concave nanocubes was  $11.3 \text{ s}^{-1}$ , which was almost four times that of the conventional Pd nanocubes ( $3.2 \text{ s}^{-1}$ ). Again, this enhanced activity could be attributed to the high density of stepped atoms (and hence active sites) on the surface of a concave nanocube.

Proton-exchange membrane (PEM) fuel cells provide an efficient and clean energy source for applications in automobiles and portable electronics, as well as on-site power generation. The development of highly active electrocatalysts for the oxygen reduction reaction (ORR) at cathode is one of the technical challenges for the successful introduction of PEM fuel cells into commercial markets. In a recent study, we evaluated the Pt concave nanocubes enclosed by {720} (see Section 4.2) as an electrocatalyst for ORR in comparison with Pt nanocubes, cuboctahedrons, and commercial Pt/C catalysts.<sup>[33]</sup> The specific activity (that is, kinetic current per unit ECSA) of the concave nanocubes was almost three and two times, respectively, greater than those of the conventional Pt nanocubes and cuboctahedrons in the potential region from 0.8 to 0.95 V (Figure 13a), demonstrating again that the important role of high-index facets in enhancing the catalytic activity for ORR. In comparison with the commercial catalyst, the Pt concave nanocubes also exhibited a specific activity more than three times higher than the 3.2 nm Pt nanoparticles in a typical Pt/C catalyst at 0.9 V (Figure 13b). These results suggest that the Pt nanocrystals with concave surfaces show promise to serve as the next-generation ORR electrocatalysts in PEM fuel cells. However, the mass activity (that is, kinetic current per unit mass of Pt) of the concave nanocubes was still less than that of the Pt/C catalyst owing to their relatively larger size and thus a smaller portion of active Pt atoms on the surface. Such a problem can be solved by reducing the size of the Pt concave nanocubes or by depositing Pt as a monolayer on concave nanocubes made of a cheaper metal (for example Pd, whose current price is only one third of that for Pt).



**Figure 13.** Comparison of electrocatalytic activities of the Pt concave cubes, cubes, and cuboctahedrons for the oxygen reduction reaction: a) specific activity given as kinetic current density ( $j_k$ ) normalized to the electrochemically active surface area (ECSA) of the catalyst, and b) specific activity of the catalyst at 0.9 V versus a reversible hydrogen electrode (RHE). For all catalysts, the metal loading on the glassy carbon electrode was  $15.3 \mu\text{g cm}^{-2}$ .<sup>[33]</sup>

## 6. Summary and Outlook

Maneuvering the shape and thus the facets and curvature of noble-metal nanocrystals has long been considered as a powerful means for tailoring their properties and enhancing their performance in a wide variety of applications. Significant progress has been made in recent years with regard to the synthesis of noble-metal nanocrystals with flat or convex surfaces under both thermodynamically and kinetically controlled conditions. In contrast, synthesis of noble-metal nanocrystals with concave surfaces is still at a very early stage of development owing to the involvement of high-index facets and negative surface curvature with high surface energies. Nevertheless, it has become clear that high-index facets other than {100}, {111}, and {110} are of great importance in improving the activity and selectivity of noble-metal nanocrystals for a given catalytic reaction because of the presence of low-coordinate atomic steps and kinks at high densities. Owing to the negative curvature and possible sharp features on the surface, it is also expected that concave nanocrystals will find widespread use in a range of applications beyond catalysis, including surface plasmon resonance, surface-enhanced spectroscopy, and optical sensing.

Herein, we have discussed a number of synthetic strategies based on selective etching, galvanic replacement, surface capping, kinetic control, and template direction that have

been used to control the formation of noble-metal nanocrystals with concave surfaces in a solution phase. We have strived to build a connection between the shape or morphology taken by a nanocrystal and the experimental parameters and thus shed light on the growth mechanism. Ultimately, the mechanistic understanding will provide some guidelines for the design of a synthesis to generate concave nanocrystals with desired compositions, facets, and properties. It is expected that the synthesis and utilization of noble-metal nanocrystals with concave surfaces will keep advancing at an accelerated speed as deeper understanding and better control of the growth mechanism and structure–property relationships become available.

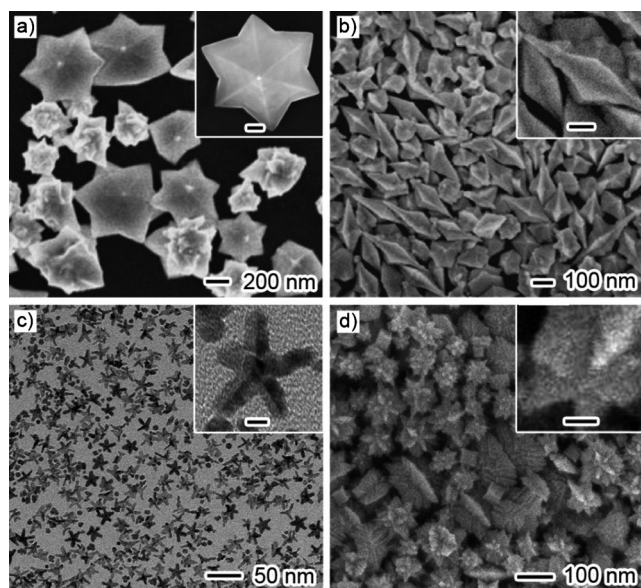
Parallel to the extensive work on concave noble-metal nanocrystals with a single-crystal structure, synthesis of twinned nanocrystals with concave surfaces have also started to appear in recent years.<sup>[77–81]</sup> For example, hexagram-shaped nanoparticles of Au (Figure 14a), fivefold-branched nanocrystals of Au (Figure 14b), starfish-like nanocrystals of Rh (Figure 14c), and sea urchin-like nanorods of Pd (Figure 14d) have all been successfully synthesized by methods based on seeded overgrowth, which could be controlled by manipulating reaction conditions such as the type and concentration of capping agents and precursors. Like their single-crystal counterparts, these twinned nanocrystals with concave surfa-

ces were derived from seeds with different numbers of defects that might include stacking faults, singly-twinned planes, and multiply-twinned planes. As such, the internal structure of the corresponding seed (that is, the number of twin defects included) plays a critical role in determining the crystallinity (for example, single crystals or twinned) of a product, and thus its final morphology. The availability of nanocrystals with concave surfaces and twinned structures is of great importance not only in expanding the diversity of concave nanocrystals but also in provide an additional handle to tailor/enhance their properties for a variety of applications such as catalysis and electrocatalysis.

*This work was supported in part by grants from NSF (DMR, 1104614 and 1215034), a DOE subcontract from the University of Delaware (DE-FG02-03 ER15468), and startup funds from Georgia Institute of Technology. During the preparation of this review article, Y.X. was also supported in part by the World Class University (WCU) Program at Yonsei University and LG Display International Collaboration Program. As a visiting scientist in the Xia group, H.Z. was also partially supported by the “New Star Program” of Zhejiang University. As a visiting Ph.D. student in the Xia group from Xiamen University, M.J. was also partially supported by the China Scholarship Council (CSC).*

Received: February 26, 2012

Published online: May 25, 2012



**Figure 14.** Various types of twinned noble-metal nanocrystals with concave structures on the surface: a) hexagram-shaped particles of Au prepared by reducing  $\text{H}[\text{AuCl}_4]$  with ascorbic acid in the presence of poly(diallyldimethylammonium chloride). (Modified with permission from Ref. [77], copyright 2011 Tsinghua University Press and Springer-Verlag Berlin Heidelberg); b) five-armed particles of Au prepared by manipulating the concentration of  $\text{Br}^-$  ions in the presence of  $\text{Ag}^+$  ions (modified with permission from Ref. [78], copyright 2009 American Chemical Society); c) starfish-like nanocrystals of Rh prepared using polyol reduction with  $[\{\text{Rh}(\text{CF}_3\text{COO})_2\}_2]$  as a chloride-free precursor;<sup>[79]</sup> d) sea urchin-like particles of Pd obtained using both sodium citrate and cetyltrimethylammonium bromide (CTAB) as capping agents. (Modified with permission from Ref. [80], copyright 2009 Chinese Physical Society.)

- [1] Y. Yin, A. P. Alivisatos, *Nature* **2005**, 437, 664.
- [2] S. G. Kwon, T. Hyeon, *Acc. Chem. Res.* **2008**, 41, 1696.
- [3] Y. W. Jun, J. S. Choi, J. Cheon, *Angew. Chem.* **2006**, 118, 3492; *Angew. Chem. Int. Ed.* **2006**, 45, 3414.
- [4] C. Burda, X. B. Chen, R. Narayanan, M. A. El-Sayed, *Chem. Rev.* **2005**, 105, 1025.
- [5] Y. Xia, Y. J. Xiong, B. Lim, S. E. Skrabalak, *Angew. Chem.* **2009**, 121, 62; *Angew. Chem. Int. Ed.* **2009**, 48, 60.
- [6] B. Lim, M. J. Jiang, J. Tao, P. H. C. Camargo, Y. M. Zhu, Y. Xia, *Adv. Funct. Mater.* **2009**, 19, 189.
- [7] A. R. Tao, S. Habas, P. D. Yang, *Small* **2008**, 4, 310.
- [8] J. E. Millstone, S. J. Hurst, G. S. Metraux, J. I. Cutler, C. A. Mirkin, *Small* **2009**, 5, 646.
- [9] X. Z. Wang, Z. B. Zhao, J. Y. Qu, Z. Y. Wang, J. S. Qiu, *Cryst. Growth Des.* **2010**, 10, 2863.
- [10] J. H. Li, W. Zhou, M. Yao, L. Guo, Y. M. Li, S. H. Yang, *J. Am. Chem. Soc.* **2009**, 131, 2959.
- [11] X. H. Liu, R. Huang, J. Zhu, *Chem. Mater.* **2008**, 20, 192.
- [12] N. Berkovitch, P. Ginzburg, M. Orenstein, *Nano Lett.* **2010**, 10, 1405.
- [13] N. Tian, Z. Y. Zhou, S. G. Sun, *J. Phys. Chem. C* **2008**, 112, 19801.
- [14] S. W. Lee, S. O. Chen, W. C. Sheng, N. Yabuuchi, Y. T. Kim, T. Mitani, E. Vescovo, Y. Shao-Horn, *J. Am. Chem. Soc.* **2009**, 131, 15669.
- [15] K. Lim, Y. Xia, *Angew. Chem.* **2011**, 123, 78; *Angew. Chem. Int. Ed.* **2011**, 50, 76.
- [16] X. L. Li, G. Ouyang, G. W. Yang, *Phys. Rev. B* **2007**, 75, 245428.
- [17] B. Wiley, T. Herricks, Y. Sun, Y. Xia, *Nano Lett.* **2004**, 4, 1733.
- [18] Y. Xiong, J. Chen, B. Wiley, Y. Xia, S. Aloni, Y. Yin, *J. Am. Chem. Soc.* **2005**, 127, 7332.
- [19] S. Im, Y. Lee, B. Wiley, Y. Xia, *Angew. Chem.* **2005**, 117, 2192; *Angew. Chem. Int. Ed.* **2005**, 44, 2154.



- [20] M. J. Mulvihill, X. Y. Ling, J. Henzie, P. D. Yang, *J. Am. Chem. Soc.* **2010**, *132*, 268.
- [21] X. Xia, J. Zeng, B. Mcdearmon, Y. Zheng, Q. Li, Y. Xia, *Angew. Chem.* **2011**, *123*, 12750; *Angew. Chem. Int. Ed.* **2011**, *50*, 12542.
- [22] Y. Y. Ma, Q. Kuang, Z. Y. Jiang, Z. X. Xie, R. B. Huang, L. S. Zheng, *Angew. Chem.* **2008**, *120*, 9033; *Angew. Chem. Int. Ed.* **2008**, *47*, 8901.
- [23] Y. Yu, Q. B. Zhang, X. M. Lu, J. Y. Lee, *J. Phys. Chem. C* **2010**, *114*, 11119.
- [24] J. Zhang, M. R. Langille, M. L. Personick, K. Zhang, S. Y. Li, C. A. Mirkin, *J. Am. Chem. Soc.* **2010**, *132*, 14012.
- [25] D. Kim, T. Yu, E. Cho, Y. Ma, O. Park, Y. Xia, *Angew. Chem.* **2011**, *123*, 6452; *Angew. Chem. Int. Ed.* **2011**, *50*, 6328.
- [26] Y. Xiong, B. Wiley, J. Chen, Z. Y. Li, Y. Yin, Y. Xia, *Angew. Chem.* **2005**, *117*, 8127; *Angew. Chem. Int. Ed.* **2005**, *44*, 7913.
- [27] X. Q. Huang, S. H. Tang, H. H. Zhang, Z. Y. Zhou, N. F. Zheng, *J. Am. Chem. Soc.* **2009**, *131*, 13916.
- [28] M. S. Jin, H. Zhang, Z. X. Xie, Y. Xia, *Angew. Chem.* **2011**, *123*, 7996; *Angew. Chem. Int. Ed.* **2011**, *50*, 7850.
- [29] J. T. Ren, R. D. Tilley, *J. Am. Chem. Soc.* **2007**, *129*, 3287.
- [30] S. Cheong, J. Watt, B. Ingham, M. F. Toney, R. D. Tilley, *J. Am. Chem. Soc.* **2009**, *131*, 14590.
- [31] X. Q. Huang, Z. P. Zhao, J. M. Fan, Y. M. Tan, N. F. Zheng, *J. Am. Chem. Soc.* **2011**, *133*, 4718.
- [32] T. Herricks, J. Y. Chen, Y. Xia, *Nano Lett.* **2004**, *4*, 2367.
- [33] T. Yu, D. Y. Kim, H. Zhang, Y. Xia, *Angew. Chem.* **2011**, *123*, 2825; *Angew. Chem. Int. Ed.* **2011**, *50*, 2773.
- [34] H. Zhang, W. Y. Li, M. S. Jin, J. E. Zeng, T. K. Yu, D. R. Yang, Y. Xia, *Nano Lett.* **2011**, *11*, 898.
- [35] C. L. Lu, K. S. Prasad, H. L. Wu, J. A. A. Ho, M. H. Huang, *J. Am. Chem. Soc.* **2010**, *132*, 14546.
- [36] C. J. DeSantis, A. A. Peverly, D. G. Peters, S. E. Skrabalak, *Nano Lett.* **2011**, *11*, 2164.
- [37] F. Wang, C. H. Li, L. D. Sun, H. S. Wu, T. A. Ming, J. F. Wang, J. C. Yu, C. H. Yan, *J. Am. Chem. Soc.* **2011**, *133*, 1106.
- [38] Y. Yu, Q. B. Zhang, B. Liu, J. Y. Lee, *J. Am. Chem. Soc.* **2010**, *132*, 18258.
- [39] H. Zhang, M. S. Jin, J. G. Wang, W. Y. Li, P. H. C. Camargo, M. J. Kim, D. R. Yang, Z. X. Xie, Y. Xia, *J. Am. Chem. Soc.* **2011**, *133*, 6078.
- [40] S. A. Bradford, *Corrosion Control*, 2nd ed., CASTI, Edmonton, **2001**, pp. 1–51.
- [41] J. Y. Chen, T. Herricks, Y. Xia, *Angew. Chem.* **2005**, *117*, 2645; *Angew. Chem. Int. Ed.* **2005**, *44*, 2589.
- [42] A. Tao, P. Sinsermsuksakul, P. D. Yang, *Angew. Chem.* **2006**, *118*, 4713; *Angew. Chem. Int. Ed.* **2006**, *45*, 4597.
- [43] H. L. Nigg, L. P. Ford, R. I. Masel, *J. Vac. Sci. Technol. A* **1998**, *16*, 3064.
- [44] S. E. Skrabalak, J. Y. Chen, Y. G. Sun, X. M. Lu, L. Au, C. M. Cobley, Y. Xia, *Acc. Chem. Res.* **2008**, *41*, 1587.
- [45] C. M. Cobley, Y. Xia, *Mater. Sci. Eng. R* **2010**, *70*, 44.
- [46] G. Z. Cao, *Nanostructures and Nanomaterials: Synthesis Properties, and Applications*, Imperial College, London, **2004**, pp. 26–31.
- [47] B. Wiley, Y. G. Sun, B. Mayers, Y. Xia, *Chem. Eur. J.* **2005**, *11*, 454.
- [48] B. J. Wiley, Y. C. Chen, J. M. McLellan, Y. J. Xiong, Z. Y. Li, D. Ginger, Y. Xia, *Nano Lett.* **2007**, *7*, 1032.
- [49] B. Lim, H. Kobayashi, P. H. C. Camargo, L. F. Allard, J. Y. Liu, Y. Xia, *Nano Res.* **2010**, *3*, 180.
- [50] C. Tsung, J. N. Kuhn, W. Huang, C. Aliaga, G. A. Somorjai, P. Yang, *J. Am. Chem. Soc.* **2009**, *131*, 5816.
- [51] Y. W. Zhang, M. E. Grass, J. N. Kuhn, F. Tao, S. E. Habas, W. Y. Huang, P. D. Yang, G. A. Somorjai, *J. Am. Chem. Soc.* **2008**, *130*, 5868.
- [52] J. Zeng, Y. Q. Zheng, M. Rycenga, J. Tao, Z. Y. Li, Q. A. Zhang, Y. M. Zhu, Y. Xia, *J. Am. Chem. Soc.* **2010**, *132*, 8552.
- [53] Y. J. Xiong, J. M. McLellan, Y. D. Yin, Y. Xia, *Angew. Chem.* **2007**, *119*, 804; *Angew. Chem. Int. Ed.* **2007**, *46*, 790.
- [54] X. Yin, X. Q. Min, Y. W. Zhang, C. H. Yan, *J. Am. Chem. Soc.* **2011**, *133*, 3816.
- [55] X. Q. Huang, S. H. Tang, X. L. Mu, Y. Dai, G. X. Chen, Z. Y. Zhou, F. X. Ruan, Z. L. Yang, N. F. Zheng, *Nat. Nanotechnol.* **2011**, *6*, 28.
- [56] C. Wang, H. Daimon, Y. Lee, J. Kim, S. Sun, *J. Am. Chem. Soc.* **2007**, *129*, 6974.
- [57] Y. J. Kang, X. C. Ye, C. B. Murray, *Angew. Chem.* **2010**, *122*, 6292; *Angew. Chem. Int. Ed.* **2010**, *49*, 6156.
- [58] J. B. Wu, A. Gross, H. Yang, *Nano Lett.* **2011**, *11*, 798.
- [59] T. K. Sau, C. J. Murphy, *J. Am. Chem. Soc.* **2004**, *126*, 8648.
- [60] J. L. Elechiguerra, J. Reyes-Gasga, M. J. Yacaman, *J. Mater. Chem.* **2006**, *16*, 3906.
- [61] M. Z. Liu, P. Guyot-Sionnest, *J. Phys. Chem. B* **2005**, *109*, 22192.
- [62] T. Ming, W. Feng, Q. Tang, F. Wang, L. D. Sun, J. F. Wang, C. H. Yan, *J. Am. Chem. Soc.* **2009**, *131*, 16350.
- [63] M. S. Jin, H. Zhang, Z. X. Xie, Y. Xia, *Energy Environ. Sci.* **2012**, *5*, 6352.
- [64] N. V. Petrova, I. N. Yakovkin, *Surf. Sci.* **2005**, *578*, 162.
- [65] A. M. Bittner, J. Wintterlin, B. Beran, G. Ertl, *Surf. Sci.* **1995**, *335*, 291.
- [66] J. B. Hunson, *Surface Science: An Introduction*, Wiley, New York, **1998**, pp. 289–304.
- [67] M. S. Jin, H. Y. Liu, H. Zhang, Z. X. Xie, J. Y. Liu, Y. Xia, *Nano Res.* **2011**, *4*, 83.
- [68] S. C. Srivastava, L. Newman, *Inorg. Chem.* **1966**, *5*, 1506.
- [69] D. Kim, Y. W. Lee, S. B. Lee, S. W. Han, *Angew. Chem.* **2012**, *124*, 163; *Angew. Chem. Int. Ed.* **2012**, *51*, 159.
- [70] L. Zhang, J. W. Zhang, Q. Kuang, S. F. Xie, Z. Y. Jiang, Z. X. Xie, L. S. Zheng, *J. Am. Chem. Soc.* **2011**, *133*, 17114.
- [71] F. R. Fan, D. Y. Liu, Y. F. Wu, S. Duan, Z. X. Xie, Z. Y. Jiang, Z. Q. Tian, *J. Am. Chem. Soc.* **2008**, *130*, 6949.
- [72] M. S. Jin, H. Zhang, J. G. Wang, X. L. Zhong, N. Lu, Z. Y. Li, Z. X. Xie, M. J. Kim, Y. Xia, *ACS Nano* **2012**, *6*, 2566.
- [73] Y. H. Bing, H. S. Liu, L. Zhang, D. Ghosh, J. J. Zhang, *Chem. Soc. Rev.* **2010**, *39*, 2184.
- [74] A. C. Chen, P. Holt-Hindle, *Chem. Rev.* **2010**, *110*, 3767.
- [75] N. Semagina, L. Kiwi-Minsker, *Catal. Rev. Sci. Eng.* **2009**, *51*, 147.
- [76] N. T. S. Phan, M. Van Der Sluys, C. W. Jones, *Adv. Synth. Catal.* **2006**, *348*, 609.
- [77] Q. Jiang, Z. Jiang, L. Zhang, H. Lin, N. Yang, H. Li, D. Liu, Z. Xie, Z. Tian, *Nano Res.* **2011**, *4*, 612.
- [78] H. L. Wu, C. H. Chen, M. H. Huang, *Chem. Mater.* **2009**, *21*, 110.
- [79] H. Zhang, X. Xia, W. Li, J. Zeng, Y. Dai, D. Yang, Y. Xia, *Angew. Chem.* **2010**, *122*, 5424; *Angew. Chem. Int. Ed.* **2010**, *49*, 5296.
- [80] X. Shen, G. Wang, X. Hong, W. Zhu, *Chin. J. Chem. Phys.* **2009**, *22*, 440.
- [81] H. Liao, Y. Jiang, Z. Zhou, S. Chen, S. Sun, *Angew. Chem.* **2008**, *120*, 9240; *Angew. Chem. Int. Ed.* **2008**, *47*, 9100.